Effects of strontium doping on microstructure and functional properties of solution-derived potassium sodium niobate thin films

Katarina Vojisavljević[1,2,*], Tanja Vrabelj[1,3], Hana Uršič[1], Barbara Malič[1]

[1]*Jožef Stefan Institute, Electronic Ceramics Department, Jamova cesta 39, 1000 Ljubljana, Slovenia*
[2]*Institute for Multidisciplinary Research, University of Belgrade, Department of Materials Science, Kneza Višeslava 1, 11030 Belgrade, Serbia*
[3]*University of Maribor, Faculty of Chemistry and Chemical Engineering, Smetanova ulica 17, 2000 Maribor, Slovenia*

Abstract

The effects of strontium doping (0–2 mol%) on structure, microstructure and functional properties of potassium sodium niobate (KNN) thin films deposited on Pt(111)/TiO$_x$/SiO$_2$/Si substrates were investigated. Incorporation of Sr up to 1 mol% into the KNN crystal lattice hindered the grain growth, vertical roughness and contributed to the fine-grained and dense thin film microstructure with monoclinic crystal syngony. This effectively reduced leakage current and improved ferroelectric characteristics. Higher doping content (2 mol%) led to the formation of secondary phases and complete deterioration of functional properties. Stabilization of 1 mol% Sr-doped KNN solution with diethanolamine resulted in the film with dielectric constant and losses of 394 and 0.018 at 100 kHz, respectively, leakage current of $3.8 \cdot 10^{-8}$ A/cm^2 at 100 kV/cm and well saturated ferroelectric hysteresis with P_r of 6.8 μC/cm^2 and low E_c of 85 kV/cm. Benefiting from improved leakage current characteristics at high electric fields and less defect structure, the film showed maximal local piezoelectric coefficient, $d_{33} \sim$ 110 pm/V determined by piezo-response force microscopy (PFM), ability to reach fully saturated local hysteresis under low switching DC voltage of 15 V, and good ferroelectric domain mobility proven by successful in-situ poling of chosen area using PFM lithography.

Keywords: KNN films, doping, microstructure, ferroelectric properties, piezoelectric properties

I. Introduction

Potassium sodium niobate, $K_{0.5}Na_{0.5}NbO_3$ (KNN), is the one of the most intriguing and often investigated lead-free materials with reversible hysteretic dependence of polarization under applied electric field, with orthorhombic/monoclinic symmetry at room temperature and phase transitions (rhombohedral (R) $\rightarrow$ orthorhombic/monoclinic (O/M) $\rightarrow$ tetragonal (T) $\rightarrow$ cubic (C), with corresponding transition temperatures $T_{R\text{-}O/M} \sim -153$ °C, $T_{O/M\text{-}T} \sim 200$ °C and $T_C \sim 420$ °C) similar to those in BaTiO$_3$. It possesses a piezoelectric coefficient $d_{33} \sim$ 80–160 pC/N, and in contrast to BaTiO$_3$, a high Curie temperature, T_C of ~420 °C [1–4].

Since the miniaturization has become an important

measure of technological advancement in the field of microelectromechanical systems, energy harvesters and sensors, the interest for the piezoelectric materials in thin film form has rapidly increased. Although the latest results on piezoelectric activity of KNN ceramics revealed that this material can compete with lead-based ones, certain concerns with regard to quality and possible application of KNN-based films in miniaturized devices still exist. No matter if they are processed by one of the physical or chemical vapour deposition methods or derived from chemical solutions, their functional properties can be hardly compared to the ceramic counterparts. A leaky polarization vs. electric field dependence and low piezoelectric activity, usually reported for solution derived KNN films [5,6], could be related to the large leakage current that can arise from the emergence of alkali and oxygen vacancies and moisture sensitive secondary phases, all induced by

*Corresponding author: tel: +381 11 3055 289,
e-mail: kvojisavljevic@imsi.bg.ac.rs*

the volatilization of alkaline species during heating. In spite that the sol gel method provides a variety of options to overcome such problems, namely through adjustment of solution chemistry (choice of reagents, use of chelating agents), alkali excess and chemical modification, or even through the impact on thin film orientation and microstructure, some remarkable improvement in functional properties has been rarely observed. The films derived from the KNN sols with 10 mol% K and Na excess resulted in saturated hysteresis loops with $2P_r \sim 14 \mu C/cm^2$, $2E_c \sim 140 kV/cm$ and effective piezoelectric coefficient, d_{33} of 46 pm/V measured by the scanning-probe microscope, SPM [6]. A large effective piezoelectric coefficient, d_{33} of 83 pm/V was demonstrated for the KNN films derived from solutions in which the combination of ethylenediaminetetraacetic acid-diethanolamine-monoethanolamine stabilizing chemical agents was introduced to supress the loss of volatile alkali species and reduce the leakage current [7]. On the other hand, the shifting of T_{O-T} phase transition to room temperature by Li- and Ta- modification of the KNN films followed by reduction of the leakage current density due to simultaneous co-doping with Mn allowed a significant improvement in ferroelectric properties ($P_r = 16.1 \mu C/cm^2$, $E_c = 22.2 kV/cm$) and resulted in local piezoelectric coefficient, d_{33} of 61 pm/V [8]. In 2009, one of the rare examples of an excellent local piezoelectric coefficient, d_{33} of 192 pm/V measured by the SPM with a conductive Rh-coated Si tip in the piezoresponse mode was reported by Li *et al.* [9] for the KNN films with 6 mol% Li introduced as an equipollent A-site dopant. The same author recently investigated the thermally induced domain evolution in a high-quality epitaxial Li-doped KNN/STO(001) thin films suggesting that the enhanced piezoelectric response observed across the thermotropic phase boundary can be associated with a change in structure from a typical monoclinic M_C (cubic-like) to a monoclinic M_A one (tetragonal-like, $c > a$) [10]. However, the influence of the partial replacement of A-site ions from the perovskite KNN lattice with aliovalent dopants, and especially with alkaline-earths, on functional properties of the sol-gel derived KNN films has been scarcely investigated. To the best of our knowledge, the changes in microstructure, electrical and piezoelectric properties were followed only in Mn-doped $(1-x)K_{0.5}Na_{0.5}NbO_3$-$xCaZrO_3$, ($x = 0, 0.05, 0.1$ mol) thin films, where adding CaZrO$_3$ up to 10 mol% was effective in achieving of a dense microstructure with small grains <100 nm, while Mn co-doping contributed to improved leakage current properties. The $0.95K_{0.5}Na_{0.5}NbO_3$-$0.5CaZrO_3$ composition with 1 mol% Mn showed the highest effective piezoelectric coefficient, d_{33} of 32 pm/V measured by the double beam laser interferometer [11]. Unfortunately, the individual doping effect of Ca or other alkaline earths on microstructure and functional properties of KNN thin films were not commented in literature.

From that point of view, the purpose of this study is to examine the Sr-doping effect on microstructure, dielectric, ferroelectric and leakage current properties of the KNN thin films, and to determine the optimum Sr-doping amount. Single-phase films are derived from the alkali-acetate and niobium ethoxide based solutions. It is shown that 1 mol% Sr is sufficient to reduce the leakage current due to the electron-hole recombination and improve the ferroelectric properties of the KNN film. In addition, the role of diethanolamine as a stabilizing agent in improvement of functional properties of the KNN film with 1 mol% Sr is presented. The low voltage induced polarization switching and a distinct local piezoresponse with a maximum value of ~110 pm/V suggest that piezoelectric properties of KNN thin films can be boosted through Sr-doping and adjustment of solution chemistry.

II. Synthesis and methods

For the processing of KNN sols with the nominal composition $(K_{0.5}Na_{0.5})_{1-x}Sr_xNbO_3$, $x = 0$, 0.005, 0.01 and 0.02, the following reagents were used: potassium acetate (CH$_3$COOK, ≥99%, Sigma-Aldrich), sodium acetate (CH$_3$COONa, 99.9%, ChemPur), water-free strontium acetate ((CH$_3$COO)$_2$Sr, 99.81%, Alfa Aesar) and niobium pentaethoxide ((CH$_3$CH$_2$O)$_2$Nb, 99.99%, Alfa Aesar). The 2-methoxyethanol (CH$_3$OCH$_2$CH$_2$OH, anhydrous, 99.8%, Sigma-Aldrich) was selected as a solvent for all reagents except for the strontium acetate, where glacial acetic acid (CH$_3$COOH, 100%, Merck) was chosen for its dissolution at room temperature.

All steps involved in processing of 0.2 M KNN sols are schematically presented in Fig. S1 and explained in Electronic Supporting Information (ESI, Section S1, Fig. S1). In some experiments, diethanolamine (DEA: HN(CH$_2$CH$_2$OH)$_2$, 99%, Alfa Aesar) was introduced in Nb:DEA = 1:2 molar ratio to the system in order to stabilize niobium pentaethoxide through the formation of a cage-like ligand. The procedure is explained in ESI, Section S1.

The approximately 250 nm thick Sr-doped KNN thin films on Pt(111)/TiO$_y$/SiO$_2$/Si substrates were obtained through eight repeated spin-coating, drying (150 °C/2 min) and pyrolysis steps (300 °C/2 min) followed by the rapid thermal annealing of the last deposited layer at 650 °C in air for 5 min with heating and cooling rates of 12 °C/s.

All sols and films were denoted as KNN$_S$-xSr and KNN$_F$-xSr (S - sol, F - thin film, x = 0, 0.5, 1 and 2 corresponding to the concentration of Sr in mol%), respectively, while in the case of chemical modification with diethanolamine, the abbreviation DEA was added at the end of the product name.

The X-ray powder diffraction (XRD) patterns were recorded by X-ray powder diffractometer (PANalytical X'Pert PRO MPD, Almelo, the Netherlands) by using the monochromatic CuK$_{\alpha 1}$ radiation ($\lambda = 0.15406$ nm)

with an operating voltage of 45 kV and current of 40 mA in the angular range $2\theta = 10–65°$, with a step scan $\Delta(2\theta) = 0.034°$ and integration time of 100 s, and further analysed by Jana2006 software. The background was modelled by Legendre polynomial function, a shift correction was made, and the lattice parameters were obtained from the peak positions and Miller indices of monoclinic structure.

The microstructures of the films' surfaces and cross-sections were analysed by the field emission scanning electron microscope, FE-SEM (JEOL JSM7600F, Tokyo, Japan) operating in secondary electron imaging mode at accelerating voltage of 5 kV and at a working distance of 4.5 mm. The mean grain size in all KNN films was determined with a stereological analysis by adopting the Image Tool software, where at least two digitalized surface microstructures were processed in order to extract the Feret diameters from the areas (4 μm × 3 μm in total) with more than 700 grains.

For thermal analysis (TA), the solutions were dried at 60 °C for 30 min, at 90 °C for 60 min and at 110 °C for 60 min. The thermal decomposition of the KNN gels was followed by a thermogravimetric-differential thermal analyser (TG-DTA, NETZSCH STA 409 C/CD, NETZSCH-Gerätebau GmbH, Selb, Germany) by heating ~0.05 g of the gel in a Pt crucible to 750 °C at a heating rate of 10 °C/min in an air under a flow rate of 40 cm^3/min.

For electrical characterization, approximately 100 nm thick Cr/Au top electrodes with the diameter 0.2 mm were applied through a shadow mask onto the thin film surface by DC sputtering, and post-annealed at 400 °C for 15 min. The frequency dependent dielectric properties (Impedance analyser HP 4192A) were measured from 1 kHz to 1 MHz at room temperature. The Aix-ACCT TF Analyser 2000 was used to follow the polarization versus electric field dependence by using a triangular AC-electric field at 1 kHz and at room temperature, as well as for the evaluation of the leakage current density of films within the voltage range up to ±5 V, or up to ±10 V for the evaluation of leakage-current mechanism.

The topography-height and the piezo-response force microscope (PFM) images were recorded using an atomic force microscope (AFM; Asylum Research, Molecular Force Probe 3D, Santa Barbara, CA). The electric field was applied between conductive AFM tip and sample's bottom electrode. A Pt-coated Si tip with a radius of curvature ~10 nm (OMCL-AC240TM-R3, Olympus, Japan) was used. The spring constant and the resonance frequency of the cantilevers were 2 N/m and 70 kHz, respectively. The out-of-plane amplitude and phase PFM images were measured in the Dual AC resonance tracking (DART) mode applying AC voltage with the amplitude 1 V and frequency ~300 kHz. The local hysteresis loops were measured in the Switching spectroscopy (SS) mode with the pulse DC step signal and overlapped drive AC signal (off-loop mode; applying a pulse voltage and measuring the piezoelectric signal at zero DC bias voltage) to minimize the electrostatic interactions between the tip and the sample [12]. The waveform parameters were: the sequence of increasing DC electric field steps was 20 Hz with a maximum amplitude of 35 V or 15 V. The frequency of the triangle envelope was 0.2 Hz, with an overlapping AC sinusoidal signal of amplitude 5 V or 3 V and frequency 300 kHz. Local piezoelectric values were determined in a PFM Single frequency mode by applying AC voltage with the amplitude 1 V and frequency 280 kHz, which is approximately 30 kHz below the contact resonant frequency (off-resonance measurement). The most commonly measured local d_{33}^{eff} value was determined from PFM maps by program Gwyddion 2.41. Prior to measurements the PFM response was tested by standard quartz sample (SiO$_2$ crystal, x-cut, MTI Corporation, Richmond, CA, US) with the known piezoelectric coefficient. *In-situ* poling experiment was done by PFM lithography mode using a square pattern divided to two halves. In each half the DC voltage of the opposite sign was applied. DC poling voltages of ±12 V, ±16 V and ±25 V were applied on the same area of thin-film samples with intermediate PFM scanning by AC voltage with the amplitude 3 V and frequency 300 kHz.

III. Results

3.1. Structure and microstructure of Sr-doped KNN thin films

In order to follow the influence of the Sr-doping content (0, 0.5, 1 and 2 mol%) on the phase composition of the KNN thin films deposited onto Pt/TiO$_x$/SiO$_2$/Si substrates and thermally treated at 650 °C for 5 min, the XRD patterns are collected and presented in Fig. 1a. All films up to 1 mol% Sr crystallize in a pure perovskite structure without secondary phases and they all possess {100} preferential orientation. While the preferential orientation is still present in KNN$_F$-2Sr, the small reflection detected at 28.914° 2θ indicates the appearance of the trace amount of secondary K$_3$NbO$_4$ phase (cubic F23, PDF 00-052-1895). Except of the slight asymmetry, a splitting of the {h00} reflections at ~22° and ~46°, which is typical for the KNN powder with monoclinic structure (cell parameters: $a = 0.40046$ nm, $b = 0.39446$ nm, $c = 0.40020$ nm and $\beta = 90.333°$, [24]), was not observed in Fig. 1a. Such appearance is connected with a small crystallite size and fine-grained structure [13]. A closer inspection of the {100} reflection at ~22° in XRD patterns of KNN$_F$-xSr films (Fig. 1b) confirms its systematic upshift with the increase of Sr doping content from 0 to 2 mol%. A slight broadening and progress in reduction of the {100} peak asymmetry are also observed and they can be connected with lattice distortion and decrease in crystallite size induced by Sr^{2+} incorporation into KNN crystal lattice.

A degree of the preferred orientation in the thin film samples shown in Fig. 1a was quantified by Lotgering
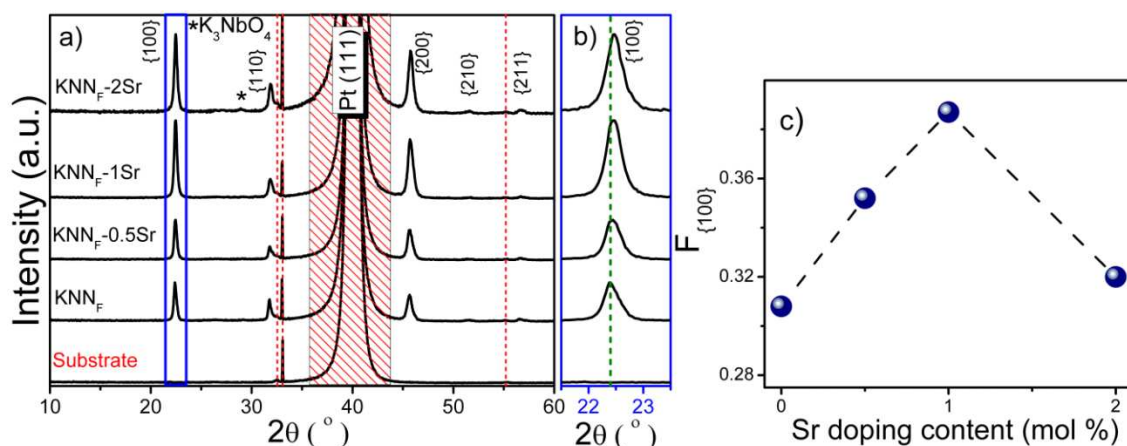
Figure 1. XRD patterns (a), evolution of the {100} reflection (b) and Lotgering factor $F_{\{100\}}$ (c) of the KNN$_F$-xSr films, annealed at 650 °C for 5 min (red dashed lines indicate positions of additional Si and Pt reflections from the substrate, while the top of {100} reflection in KNN$_F$ film is depicted by a green dashed line)

factor $F_{\{100\}}$ and presented in Fig. 1c. The observed increase from 0.30 to 0.39 with increasing amount of Sr from 0 to 2 mol% indicates that doping with Sr favours the KNN structure in which the surface energy of the {100} faces is the lowest. In addition, it was experimentally confirmed by the TG-DTA analysis (Fig. S2, ESI, Section 2), that doping with Sr decreases a crystallization temperature of the KNN films. Consequently, when the KNN$_F$-xSr films are annealed under the same conditions (650 °C/5 min), the film with 1 mol% Sr exhibits a better crystallinity and higher degree of preferred {100} orientation compared to other KNN$_F$-xSr films. Doping with 1 mol% Sr was found to be the optimum, since further increase in doping content (2 mol%) resulted in appearance of the secondary K_3NbO_4 phase and decrease in Lotgering factor to 0.32.

The cross-sectional and the surface microstructures of the KNN$_F$-xSr films along with the grain size distributions determined from the surface microstructures are presented in Fig. 2. A carefully tuned thermal treatment conditions allowed the control over the nucleation and grain growth rates, which resulted in prevailing homogeneous nucleation and fine-grained microstructure, in accordance with results of Kupec *et al.* [13]. A relatively broad grain size distribution from a few 10 nm to about 160 nm, and with an average grain size of 69.5 nm was typical for the 250 nm thick KNN$_F$ film. In contrast, the microstructures of about 240 nm and 230 nm thick KNN$_F$-0.5Sr and KNN$_F$-1Sr films reveal more uniform size distributions and decrease in average grain size to the values of 55.9 nm and 45.6 nm, respectively. The observed narrower grain size distribution and lower value
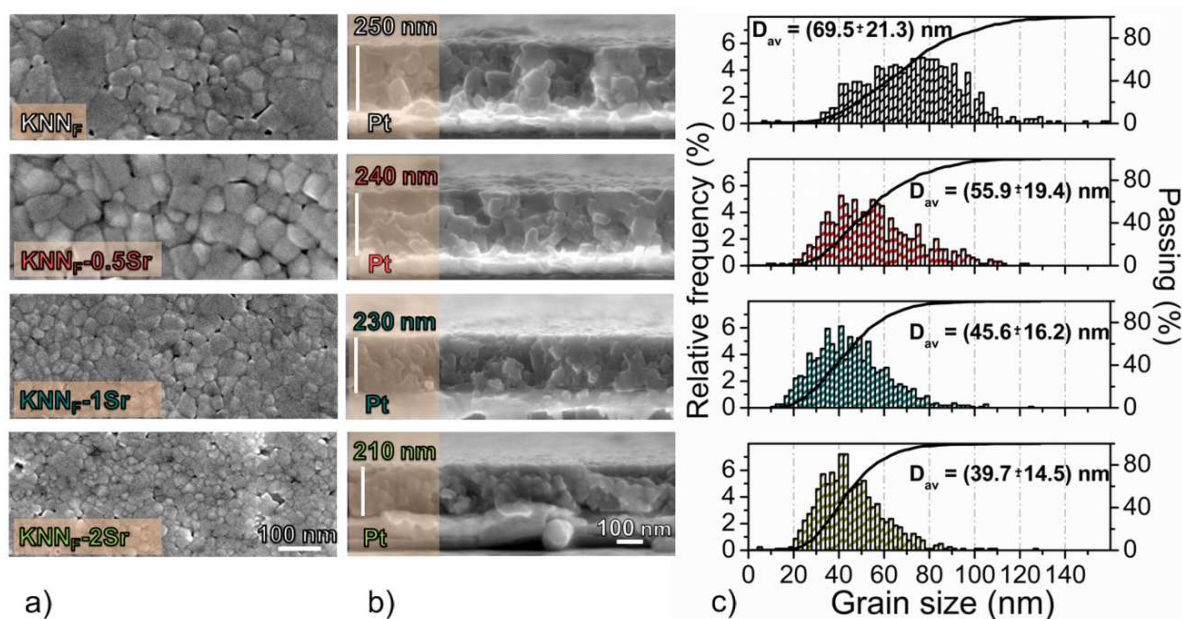
Figure 2. Surface FE-SEM (a) and cross-sectional images (b) along with the grain size distribution (c) of the KNN$_F$, KNN$_F$-0.5Sr, KNN$_F$-1Sr and KNN$_F$-2Sr films annealed at 650 °C for 5 min. KNN$_F$, KNN$_F$-0.5Sr, KNN$_F$-1Sr and KNN$_F$-2Sr micrographs of surfaces, cross-sections and corresponding grain size distribution plots are arranged in order from top to bottom in 2a-2c, respectively

Table 1. Cell parameters of KNN$_F$-xSr films annealed at 800 °C for 90 min

Sample	$a \approx c$ [nm]	b [nm]	a/b
KNN$_F$	0.3990(2)	0.3933(3)	1.0145
KNN$_F$-0.5Sr	0.3986(5)	0.3936(2)	1.0127
KNN$_F$-1Sr	0.3974(3)	0.3939(2)	1.0089
KNN$_F$-2Sr	0.3966(2)	0.3945(4)	1.0053

of the average grain size compared to the KNN$_F$ film could be related to the partial substitution of alkaline ions with Sr^{2+}, for which it was confirmed that it hinders grain growth in KNN ceramics [14–16]. Modified thermal decomposition paths of the KNN$_S$-0.5Sr and KNN$_S$-1Sr sols (Fig. S2, ESI, Section 2), i.e. observed shifting of the first thermal event toward high temperatures and subsequent shifting of the second and third thermal events toward low temperatures, obviously contributed to more narrow temperature ranges of nucleation of the KNN$_F$-0.5Sr and KNN$_F$-1Sr films compared to the KNN$_F$ film, which can additionally explain narrower grain size distributions in the doped films. As the consequence of Sr doping, the vertical roughness decreased from 15.6 nm (KNN$_F$) to 3.5 nm (KNN$_F$-1Sr), as confirmed by the AFM measurements (not shown here). A slight change in the film thicknesses from 250 nm (KNN$_F$) to 230 nm (KNN$_F$-1Sr) observed in FE-SEM cross sectional micrographs can be connected with increased Sr content, which can contribute to enhanced grain boundary mobility [14–16]. The thickness of the KNN$_F$-2Sr was even lower (210 nm) with average grain size of 39.7 nm; however, a porous microstructure was typical for this composition.

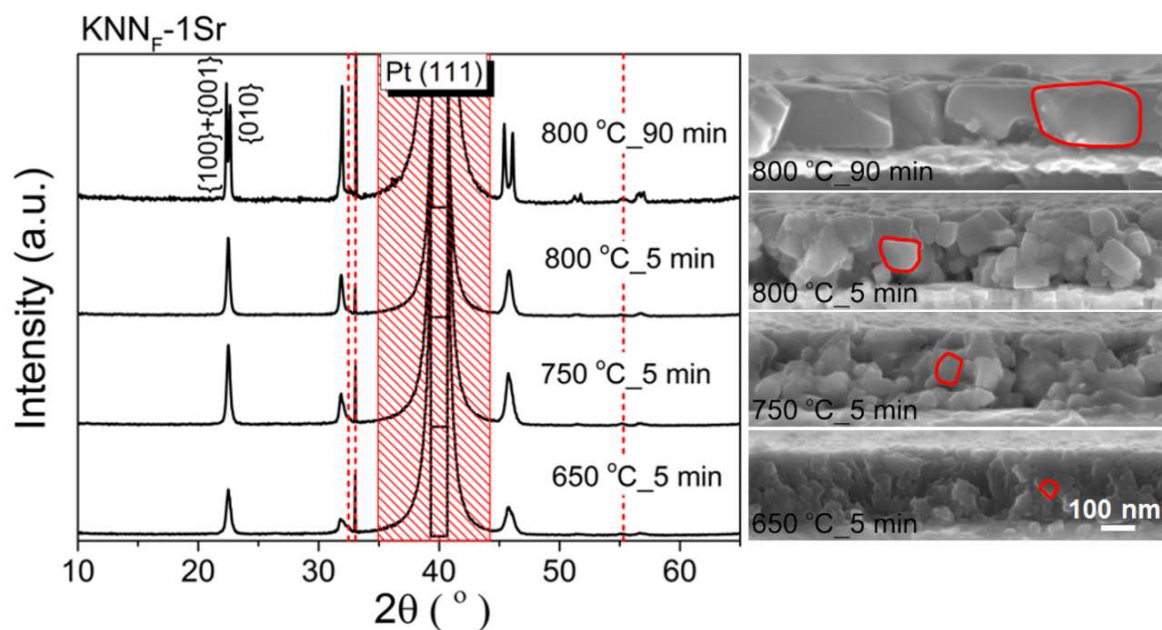In addition, the structure and microstructural changes of the KNN$_F$-xSr thin films upon heating within the temperature interval 650–800 °C and for a different holding time (5 min and 90 min) were followed, and here we pre-sented the results for the KNN$_F$-1Sr composition (see Fig. 3). The splitting of {h00} reflections was observed only in the sample annealed at 800 °C/90 min (see Fig. 3a), revealing their monoclinic structure, similar as reported by Kupec *et al.* [13]. From the positions of {100} + {001} and {010} reflections, the lattice parameters *a* and *c* were calculated, see Table 1. At the same time, the abrupt change in microstructure from a fine-grained (~50 nm) to the columnar one (~250 nm) was detected, as it was shown in Fig. 3b. In contrast to the KNN$_F$-1Sr film annealed at 650 °C/5 min, the poor functional properties of the KNN$_F$-1Sr annealed at 800 °C/90 min were detected due to the specific structure, which provided direct path for the current [13]. The similar structure and microstructural changes were observed for other KNN compositions. The *a* and *b* lattice parameters, and *a/b* ratio for all KNN$_F$-xSr thin films are shown in Table 1. An observed decrease in *a/b* ratio confirmed a pronounced tendency of the KNN$_F$-xSr films towards a pseudo-cubic structure as the result of incorporation of Sr^{2+} into the KNN crystal lattice.

3.2. Functional properties of Sr-doped KNN films

The frequency dependent dielectric properties, leakage current density (*J*) *vs.* electric field (*E*) and polarization (*P*) *vs.* electric field (*E*) of the KNN$_F$-xSr were followed and presented in Fig. 4.

The room temperature dielectric permittivity (ε')

Figure 3. XRD patterns and cross-sectional micrographs of the KNN$_F$-1Sr annealed at different temperatures and holding times, revealing the structural and microstructural changes induced by thermal treatment conditions (red dashed lines indicate positions of additional Si and Pt reflections from the substrate)
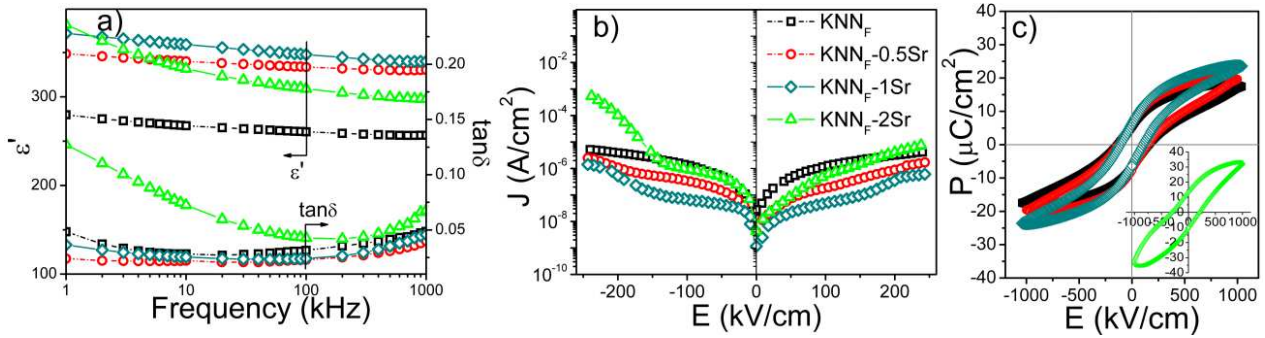
Figure 4. Dielectric properties (a) and *J-E* measurements (b) of KNN$_F$, KNN$_F$-0.5Sr, KNN$_F$-1Sr and KNN$_F$-2Sr films; *P-E* hysteresis loops of KNN$_F$, KNN$_F$-0.5Sr, KNN$_F$-1Sr (c) (the inset in 4c shows the leaky *P-E* hysteresis loop of the KNN$_F$-2Sr)

and losses (tan δ) of KNN$_F$, KNN$_F$-0.5Sr, KNN$_F$-1Sr and KNN$_F$-2Sr measured at 100 kHz are 261/0.031, 334/0.024, 347/0.022 and 309/0.042, respectively (Fig. 4a). The observed increase in ε' and decrease in tan δ up to 1 mol% Sr is in accordance with reported results on frequency dependent dielectric properties of Sr-doped KNN ceramics [10,17], and it can be attributed to improved density and narrower grain size distribution compared to the un-doped KNN$_F$ film. Further increase in Sr content (2 mol%) resulted in deterioration of microstructure and consequently in poor dielectric properties.

The Sr-doping up to 1 mol% had two significant effects on KNN thin film properties: it decreased *J* from $1.2 \cdot 10^{-6}$ A/cm^2 (KNN$_F$) to $4.6 \cdot 10^{-8}$ A/cm^2 (KNN$_F$-1Sr), both measured at the electric field of 100 kV/cm (Fig. 4b), and gave rise to improved ferroelectric behaviour of the Sr-doped KNN films. However, a relatively abrupt increase in *J* at high electric fields $E \geq 150$ kV/cm still can be seen in all films including the KNN$_F$-1Sr film with the best *J-E* characteristic (see Fig. 4b). This indicates the change in conduction mechanism, which can limit their application. The problem can be overcame by further modification of the KNN$_S$-1Sr, and it will be commented later in the text.

As it can be seen in Fig. 4c, the KNN$_F$-xSr films with Sr-doping ≤ 1 mol% possess well saturated ferroelectric hysteresis loops. Maximal values of remnant polarization (P_r) and coercive field (E_c) observed in the un-doped KNN$_F$ film were 5.5 µC/cm^2 and 157 kV/cm, respectively. The Sr-doped films up to 1 mol% showed improved ferroelectric properties, so the highest P_r of 7.2 µC/cm^2 and the lowest E_c of 102 kV/cm were measured in the KNN$_F$-1Sr film. Doping with 2 mol% Sr was exaggerated, since the leaky *P-E* loop was observed for the KNN$_F$-2Sr film (see inset in Fig. 4c).

Mechanism that lies behind reduction of E_c and leakage current can be explained by the Sr^{2+} incorporation into the KNN crystal lattice during the thermal stage of film processing. Having in mind the convenient size of Sr^{2+} ionic radius, i.e. r_{Na^+} (1.39 Å, *CN*12) $< r_{Sr^{2+}}$ (1.44 Å, *CN*12) $< r_{K^+}$ (1.64 Å, *CN*12) [14], it can replace both Na$^+$ and K$^+$ from the KNN perovskite structure and donate an extra electron, e^- to the system. This kind of doping can be compensated by the formation

of A-site vacancies during the thermal treatment, which provide the free carrier holes to the system by the following formula (Eq. 1):

$$V_{K \, or \, Na} \rightarrow V'_{K \, or \, Na} + h^+ \qquad (1)$$
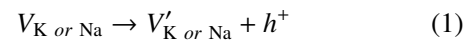
where V_K, V_{Na} are neutral K and Na vacancies, V'_K, V'_{Na} are ionized K and Na vacancies and h^+ is free carrier hole. The $e^- - h^+$ recombination leads to the decrease of conductivity and consequently contributes to the reduction of both leakage current and coercive field in the KNN$_F$-xSr films with Sr-doping ≤ 1 mol%.

In addition, the small ionic radius of Sr^{2+} compared to the ionic radius of K$^+$ most probably favours its off-center position [18] in KNN lattice. Since the Sr-donor dopant has more positive charge than the replaced K (A-site atom), it can induce the higher distortion of the structure, and it can have the positive influence on domain motion and their easier orientation under applied electric field. In addition, when the dopant concentration exceeds the concentration of the intrinsic defects in the matrix material, the introduced impurity gives rise to a compensating defect. All of these can be used to explain the enhancement of ferroelectricity in the KNN$_F$-0.5Sr and KNN$_F$-1Sr films. Similar was observed in the (1-x)(Na$_{0.5}$K$_{0.5}$)NbO$_3$-xAZrO$_3$ (A = Ca^{2+}, Sr^{2+}) solid solutions [19].

Obviously, the KNN$_F$-1Sr thin film showed the best microstructure and functional properties, thus it was chosen for further improvement.

### 3.3. Functional properties of KNN$_F$-1Sr-DEA film

Modification of KNN solutions by stabilizing chemical agents, such as polyvinilpyrrolidone, ethanolamine, diethanolamine, ethylenediamine-tetra-acetic acid, was reported to have a positive influence on microstructure and overall functional properties of KNN thin film, including leakage current density [7,20,21]. In fact, chemical modification can suppress reactivity of niobium ethoxide in hydrolysis and polycondenzation reactions through shielding of the metal atoms by non-hydrolysable ligands, and even it can suppress the evaporation of potassium and sodium due to their better immobilization into organic matrix [7].

Microstructure and functional properties of the KNN$_F$-1Sr-DEA film derived from diethanolamine sta-
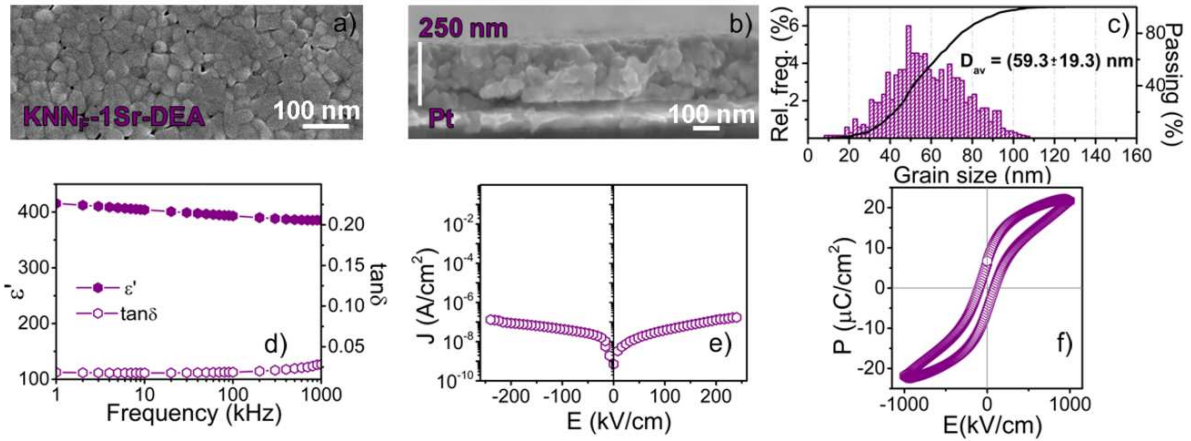
Figure 5. FE-SEM images of the surface microstructure (a) and cross-section (b) with a grain size distribution (c), dielectric properties (d) J-E measurement (e) and P-E hysteresis loop (f) of the KNN$_F$-1Sr-DEA film annealed at 650 °C for 5 min
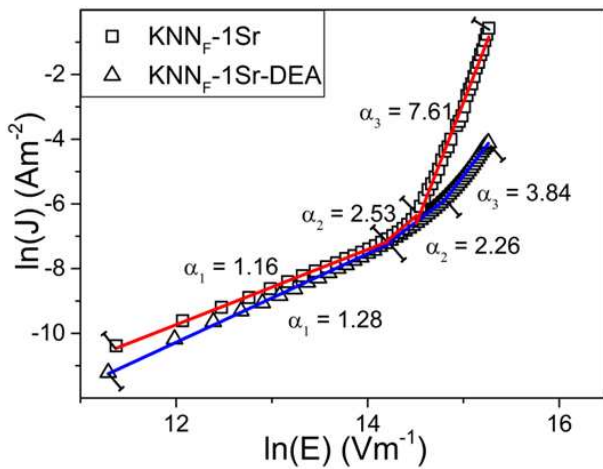
Figure 6. ln J vs. ln E characteristics for the KNN$_F$-1Sr and KNN$_F$-1Sr-DEA films (the thick solid lines correspond to the best linear-fit drawn through the experimental points (□ or △) within the fitting regions, for which the values of the slopes α_i are given)

bilized solution are presented in Fig. 5. The fine-grained microstructure with a very flat surface and narrow grain size distribution with average grain size of 59.3 nm is typical for the film (see Fig. 5a), the thickness of which is 250 nm, Fig. 5b. The microstructure with a slightly lager grains compared to KNN$_F$-1Sr film contributed to improvement of all functional properties. As it can be seen from Figs. 5c-5f, the KNN$_F$-1Sr-DEA film possesses the dielectric permittivity, ε' and dielectric loss, tan δ of 394 and 0.018 at 100 kHz, respectively, leakage current of $3.8 \cdot 10^{-8}$ A/cm^2 at 100 kV/cm and well saturated ferroelectric hysteresis loop with P_r of 6.9 μC/cm^2 and relatively low E_c of 85 kV/cm. Compared to the KNN$_F$-1Sr film, a low leakage current density of $1.6 \cdot 10^{-7}$ A/cm^2 was measured at 250 kV/cm, which is one order lower than in the KNN$_F$-1Sr measured at the same electric field.

Additionally, the leakage current mechanisms of the KNN$_F$-1Sr and KNN$_F$-1Sr-DEA films were analysed in the field range up to 500 kV/cm by plotting the experimental data with respect to space charge limited cur-

rent model (SCLC), i.e. as ln J vs. ln E (Fig. 6) [22]. As it can be seen, the experimental data reveal the linear ln J vs. ln E dependence at low and high fields and they are well fitted by the three linear segments in both cases. The low increase in conductivity up to 150 kV/cm with the slope of 1.16 (KNN$_F$-1Sr) and 1.28 (KNN$_F$-1Sr-DEA) indicates that the ohmic conduction ($J \sim \alpha E$; $\alpha \sim 1$) is the dominant factor at low fields. With further increase of the electric field, the ln J vs. ln E profiles of the films become steeper (α_2, $\alpha_3 > 2$), confirming the change in conduction mechanism to SCLC. According to the SCLC model, the free carrier concentration increases by increasing the electric field due to the injected carriers, and when the magnitude of the injected carriers is larger than its thermal equilibrium value, the conduction mechanism turns from ohmic to SCLC. The presence of the localized defect states or traps within the band gap significantly influences the transport of injected electrons and current-electric field profile. As long as the injected electrons fill all the trapping sites, shallow trap square low is dominant ($\alpha \sim 2$), and when the entire trap population is filled, further injection of carriers leads to the abrupt increase in current, and the current-electric relationship is further characterized by the trap free square low ($\alpha > 2$) [23,24]. Thus, according to SCLC theory, the steeper ln J-ln E dependence observed in the KNN$_F$-1Sr above 150 kV/cm can be correlated with its more defect structure compared to the KNN$_F$-1Sr-DEA, with large amount of A-site and oxygen vacancies, which can act as the space charge carriers, lower the barrier for carrier injection and contribute to conduction at high fields. The similar was reported for Bi(Zn$_{1/2}$Zr$_{1/2}$)O$_3$-PbTiO$_3$ films [25] and for KNN-based thin films [9,26,27].

3.4. Ferroelectric domain structure and polarization switching in KNN$_F$-1Sr and KNN$_F$-1Sr-DEA films

Local piezoelectric responses were mapped using PFM imaging as shown in Fig. 7. In the PFM amplitude images the bright regions correspond to the areas
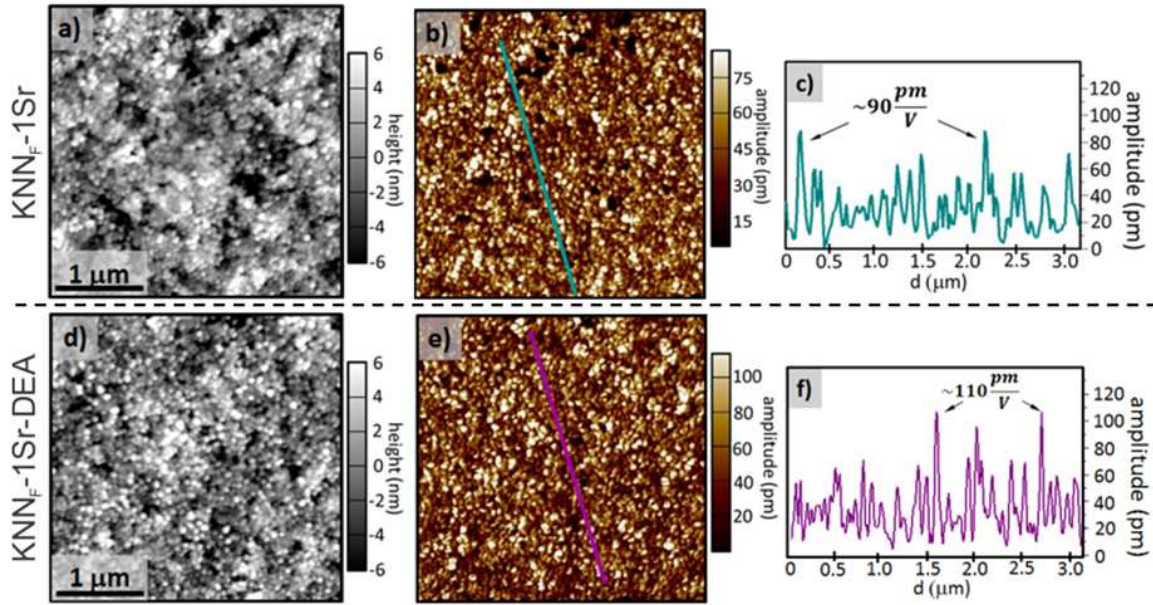
Figure 7. Topography - height image (a,d), out-of-plane PFM amplitude image (b,e) and PFM amplitude line-profiles (see lines in the panels b and e) (c,f) of the KNN$_F$-1Sr and KNN$_F$-1Sr-DEA thin films, respectively

with enhanced piezoelectric response in comparison to the dark regions. Dark regions mainly correspond to the non-active grain boundaries or porosity. At large scanning area (3 μm × 3 μm in Figs. 7b and 7e) it seems that the films contain mono-domain grains, however scanning at smaller area (1 μm × 1 μm in Figs. 7b and 7e) reveals regions of different piezo-activity inside one grain. For clarity, the inserted boxes in Fig. 7 highlight the individual grains in the topography and PFM amplitude images emphasizing regions of different piezo-activity. In these samples, the average grain size is ~50 nm, which is only ~5 times larger than radius of PFM tip. Therefore, individual domains inside grain cannot be

clearly distinguished due to the resolution limit of the PFM technique.

In order to determine the local piezoelectric coefficient d_{33}^{eff} of the prepared thin films, line-profiles were extracted as shown in Figs. 7c and 7f. Note that more than 10 line-profile analyses were made for each sample. Figure 7 contains the line-profiles with the maximum local responses (marked with arrows). The maximum response was higher in the KNN$_F$-1Sr-DEA thin film than in the KNN$_F$-1Sr thin film, namely 110 pm/V and 90 pm/V, respectively. Note that the maximum local piezoelectric coefficient d_{33}^{eff} of the KNN$_F$-1Sr-DEA was significantly higher than
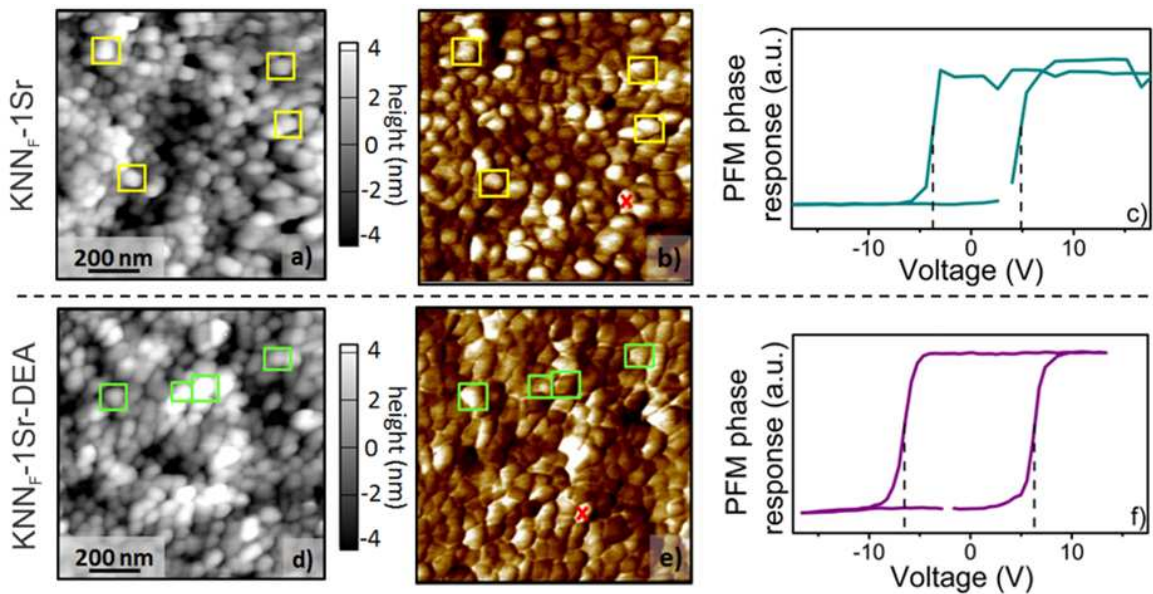

Figure 8. Topography - height image (a,d), out-of-plane PFM amplitude image (b,e) and local hysteresis loops (c,f) obtained from the areas marked by the cross in panels b and e, of the KNN$_F$-1Sr and KNN$_F$-1Sr-DEA thin films, respectively (the $\pm V_{DN}$ is marked by vertical dash lines in the panels c and f)
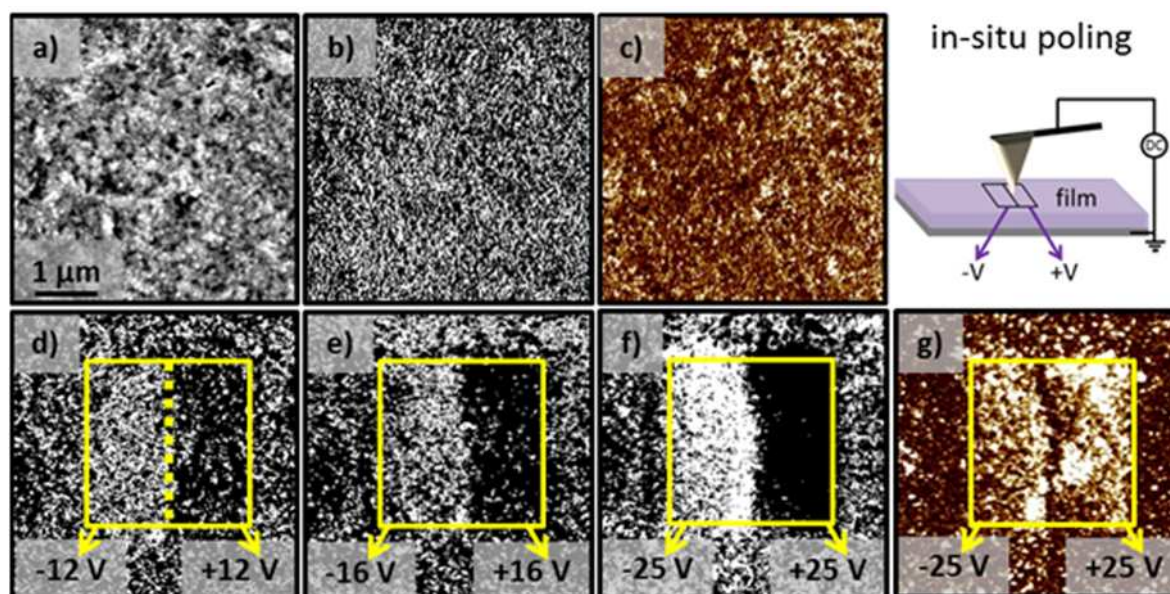
Figure 9. Topography - height image (a), PFM out-of-plane phase (b) and amplitude images (c) before *in-situ* poling experiment in KNN$_F$-1Sr-DEA thin film. PFM out-of-plane phase images (d,e,f) after applying the DC poling voltage of ±12 V, ±16 V and ±25 V, respectively and corresponding PFM out-of-plane amplitude image (g) after DC poling by ±25 V (two areas of different poling regimes (opposite sign of voltage) are marked in d by dotted line)

in $(K_{0.48}Na_{0.48}Li_{0.04})(Nb_{0.995-x}Mn_{0.005}Ta_x)O_3$ thin films [8]. Furthermore, in the KNN$_F$-1Sr films the most commonly measured local d_{33}^{eff} value is 10 pm/V, while in the KNN$_F$-1Sr-DEA films this value is 26 pm/V, which is more than 150% higher.

Examples of the local domain switching experiments are shown in Figs. 8c and 8f. In the KNN$_F$-1Sr-DEA sample the local hysteresis loops were obtained already at 15 V (maximum amplitude 15 V of pulsed DC step signal overlapped by AC sinusoidal amplitude of 3 V), while in the KNN$_F$-1Sr sample no hysteresis loops were measured at such low voltage. To obtain the local hysteresis loop in the KNN$_F$-1Sr sample higher voltage (maximum amplitude 35 V of pulsed DC step signal overlapped by AC sinusoidal amplitude of 5 V) was needed. In both samples the domain nucleation voltage (V_{DN}) is similar, namely ~5 V and ~6 V for the KNN$_F$-1Sr and KNN$_F$-1Sr-DEA sample, respectively. Therefore, all the PFM scans presented in this work were done with the AC amplitude between 1 and 3 V not to modulate the domain structure of the samples during scanning.

The result of the PFM *in-situ* poling experiment in the KNN$_F$-1Sr-DEA sample is shown in Fig. 9. A selected 5 μm × 5 μm virgin area of the sample was firstly scanned by AC amplitude of 3 V (Figs. 9a-9c). After, the 3 μm × 3 μm area was *in-situ* poled, meaning that the area was scanned with PFM tip under DC poling voltage of ±12 V (applied to the tip). This voltage is much higher than V_{DN} of the sample in order to switch the domains during poling experiment. After the *in-situ* poling the similar scanning conditions as the ones before poling were applied (Fig. 9d). The *in-situ* poling experiment was then repeated with the DC poling voltages of ±16 V and ±25 V (Figs. 9e-9g). As it can be clearly

observed in Figs. 9f and 9g, good domain mobility and successful *in-situ* poling were achieved in the prepared thin film.

High local piezoelectric coefficient and good domain mobility raise the interest for investigation of macroscopic properties of ~1 μm thick KNN$_F$-1Sr-DEA films in order to prove the quality of this lead-free material to be used as a transducer layer in energy harvesters.

IV. Conclusions

In this contribution, the effects of Sr-doping on microstructure, structure and functional properties of the $(K_{0.5}Na_{0.5})1-xSr_xNbO_3$ (KNN$_F$-xSr, $x = 0, 0.005, 0.01$ and 0.02) thin-films synthesized from alkali acetate-alkoxide based solutions, were studied. The Sr incorporation up to 1 mol% into the perovskite A-sublattice was followed by X-ray diffraction analysis, where the change of the $a \approx c$ and b lattice parameters revealed the monoclinic structure, and where the reduction of a/b ratio confirmed its tendency to pseudo-cubic syngony at higher Sr-doping levels. This kind of doping hindered the grain growth and subsequently vertical roughness of as prepared films. It contributed as well to the soft ferroelectric characteristics (KNN$_F$: $P_r = 5.5\,\mu C/cm^2$, $E_c = 157\,kV/cm$ and KNN$_F$-1Sr: $P_r = 7.2\,\mu C/cm^2$, $E_c = 102\,kV/cm$) and significant reduction of leakage component due to $e^-–h^+$ recombination induced by incorporation of Sr^{2+} into KNN crystal lattice. The doping with 1 mol% Sr was the optimum for improvement of functional properties; higher doping content (2 mol%) led to deterioration of microstructure and contributed to the high leakage component and leaky *P-E* loops. Considering the problems with high leakage current observed at high electric fields (>150 kV/cm) in the KNN$_F$-1Sr film,

an improved synthesis procedure of the KNN_S-1Sr solution with diethanolamine was of great benefit to the conduction mechanism of the KNN_F-1Sr-DEA film. The ohmic conduction was the dominant leakage current mechanism at low fields (<150 kV/cm), and it changed to the space charge limited conduction at high fields (150 kV/cm $\leq E \leq$ 500 kV/cm) in both KNN_F-1Sr and KNN_F-1Sr-DEA films. However, the less steep ln *J*-ln *E* profile of the KNN_F-1Sr-DEA at high fields, strongly confirmed a significant reduction in space charge defects (A-site and oxygen vacancies), supporting at the same time the key role of DEA in formation of less defect structure compared to the KNN_F-1Sr film. At the same time, the KNN_F-1Sr-DEA film showed high local piezoelectric coefficient, d_{33} of 110 pm/V and good domain mobility, which open the possibility for the practical application of such prepared films.

§ Electronic Supporting Information (ESI) can be downloaded using following link: https://bit.ly/3htdUHr

References

1. L. Egerton, D.M. Dillon, "Piezoelectric and dielectric properties of ceramics in the system potassium-sodium niobate", *J. Am. Ceram. Soc.*, **42** [9] (1959) 438–442.

2. R. E. Jaeger, L. Egerton, "Hot pressing of potassium-sodium niobates", *J. Am. Ceram. Soc.*, **45** [5] (1962) 209–213.

3. B. Malič, J. Koruza, J. Hreščak, J. Bernard, K. Wang, J.G. Fisher, A. Benčan, "Sintering of lead-free piezoelectric sodium potassium niobate ceramics", *Materials*, **8** [12] (2015) 8117–8146.

4. L. Dong, D.S. Stone, R.S. Lakes, "Enhanced dielectric and piezoelectric properties of $xBaZrO_3$-$(1-x)BaTiO_3$ ceramics", *J. Appl. Phys.*, **111** [8] (2012) 084107.

5. C.W. Ahn, S.Y. Lee, H.J. Lee, A. Ullah, J.S. Bae, E.D. Jeong, J.S. Choi, B.H. Park, I.W. Kim, "The effect of K and Na excess on the ferroelectric and piezoelectric properties of $K_{0.5}Na_{0.5}NbO_3$ thin films", *J. Phys. D Appl. Phys.*, **42** (2009) 215304.

6. Y. Nakashima, W. Sakamoto, T. Shimura, T. Yogo, "Chemical processing and characterization of ferroelectric (K,Na)NbO$_3$ thin films", *Jpn. J. Appl. Phys.*, **46** [10B] (2007) 6971–6975.

7. Y. Wang, K. Yao, M.S. Mirshekarloo, F.E.H. Tay, "Effects and mechanism of combinational chemical agents on solution-derived $K_{0.5}Na_{0.5}NbO_3$ piezoelectric thin films", *J. Am. Ceram. Soc.*, **99** [5] (2016) 1631–1636.

8. C.W. Ahn, H.J. Seog, A. Ullah, S.Y. Lee, J.W. Kim, S.S. Kim, M. Park, K. No, I.W. Kim, "Effect of Ta content on the phase transition and piezoelectric properties of lead-free $(K_{0.48}Na_{0.48}Li_{0.04})(Nb_{0.995-x}Mn_{0.005}Ta_x)O_3$ thin film", *J. Appl. Phys.*, **111** [2] (2012) 024110.

9. F. Lai, J.-F. Li, Z.-X. Zhu, Y. Xu, "Influence of Li content on electrical properties of highly piezoelectric (Li,K,Na)NbO$_3$ thin films prepared by sol-gel processing", *J. Appl. Phys.*, **106** [6] (2009) 064101.

10. J. Luo, W. Sun, Z. Zhou, Y. Bai, Z. J. Wang, G. Tian, D. Chen, X. Gao, F. Zhu, J.-F. Li, "Domain evolution and piezoelectric response across thermotropic phase boundary in (K,Na)NbO$_3$-based epitaxial thin films", *ACS Appl. Mater. Interfaces*, **9** [15] (2017) 13315–13322.

11. T. Matsuda, W. Sakamoto, B.-Y. Lee, T. Iijima, J. Kumagai, M. Moriya, T. Yogo, "Electrical properties of lead-free ferroelectric Mn-doped $K_{0.5}Na_{0.5}NbO_3$-CaZrO$_3$ thin films prepared by chemical solution deposition", *Jpn. J. Appl. Phys.*, **51** [9S1] (2012) 09LA03.

12. H.Y. Guo, J.B. Xu, I.H. Wilson, Z. Xie, E.Z. Luo, S. Hong, H. Yan, "Study of domain stability on $(Pb_{0.76}Ca_{0.24})TiO_3$ thin films using piezoresponse microscopy", *Appl. Phys. Lett.*, **81** [4] (2002) 715–717.

13. A. Kupec, B. Malic, J. Tellier, E. Tchernychova, S. Glinsek, M. Kosec, "Lead-free ferroelectric potassium sodium niobate thin films from solution: Composition and structure", *J. Am. Ceram. Soc.*, **95** [2] (2012) 515–523.

14. B. Malič, J. Bernard, J. Holc, M. Kosec, "Strontium doped $K_{0.5}Na_{0.5}NbO_3$ based piezoceramics", *Ferroelectrics*, **314** [1] (2005) 149–156.

15. B. Malič, J. Bernard, J. Holc, D. Jenko, M. Kosec, "Alkaline-earth doping in (K,Na)NbO$_3$ based piezoceramics", *J. Eur. Ceram. Soc.*, **25** [12] (2005) 2707–2711.

16. J. Hreščak, G. Dražić, M. Deluca, I. Arčon, A. Kodre, M. Dapiaggi, T. Rojac, B. Malič, A. Bencan, "Donor doping of $K_{0.5}Na_{0.5}NbO_3$ ceramics with strontium and its implications to grain size, phase composition and crystal structure", *J. Eur. Ceram. Soc.*, **37** (2017) 2073–2082.

17. M. Demartin Maeder, D. Damjanović, N. Setter, "Lead free piezoelectric materials", *J. Electroceram.*, **13** [1-3] (2004) 385–392.

18. G. Geneste, J.-M. Kiat, H. Yokota, Y. Uesu, F. Porcher. "Polar clusters in impurity-doped quantum paraelectric $K_{1-x}Li_xTaO_3$", *Phys. Rev. B*, **81** (2010) 144112.

19. R. Wang, H. Bando, M. Kidate, Y. Nishihara, M. Itoh, "Effects of A-site ions on the phase transition temperatures and dielectric properties of $(1-x)(Na_{0.5}K_{0.5})NbO_3$-xAZrO$_3$ solid solutions", *Jpn. J. Appl. Phys.*, **50** (2011) 09ND10.

20. L. Wang, K. Yao, W. Ren, "Piezoelectric $K_{0.5}Na_{0.5}NbO_3$ thick films derived from polyvinylpyrrolidone-modified chemical solution deposition", *Appl. Phys. Lett.*, **93** (2008) 092903.

21. P. C. Goh, Z. Chen, "Lead-free piezoelectric thin films derived from chemical solution modified with stabilizing agents", *Appl. Phys. Lett.*, **97** (2010) 102901.

22. A. Rose, "Space-charge-limited currents in solids", *Phys. Rev.*, **97** (6) (1955) 1538–1544.

23. M. Kleitz, J. Dupuy, *Electrode Processes in Solid-State Ionics: Theory and Application to Energy Conversion and Storage*, D. Reidel Publishing Company (Published in cooperation with NATO Scientific Affairs Division), Dordrecht-Holland/Boston-USA, 1975.

24. W. Chandra, L.K. Ang, K.L. Pey, C.M. Ng, "Two-dimensional analytical Mott-Gurney law for a trap-filled solid", *Appl. Phys. Lett.*, **90** (2007) 153505.

25. L. Zhang, J. Chen, H. Zhao, L. Fan, Y. Rong, J. Deng, R. Yua, X. Xing, "Large remanent polarization and small leakage in sol-gel derived $Bi(Zn_{1/2}Zr_{1/2})O_3$-$PbTiO_3$ ferroelectric thin films", *Dalton Trans.*, **42** (2013) 585–590.

26. L. Wang, W. Ren, P. Shi, X. Wu, "Structures, electric properties, and leakage current behaviors of un-doped and Mn-doped lead-free ferroelectric $K_{0.5}Na_{0.5}NbO_3$ films", *J. Appl. Phys.*, **115** (2014) 034103.

27. A. Kupec, H. Uršič, R.C. Frunǎ, E. Tchernychova, B. Malič, "Microstructure-dependent leakage-current properties of solution-derived $(K_{0.5}Na_{0.5})NbO_3$ thin films", *J. Eur. Ceram. Soc.*, **35** [13] (2015) 3507–3511.